

# Recovery of Absorption Spectra from Fourier Transform Infrared (FT-IR) Microspectroscopic Measurements of Intact Spheres

Thomas van Dijk,<sup>a</sup> David Mayerich,<sup>a</sup> P. Scott Carney,<sup>a,b</sup> Rohit Bhargava<sup>a,b,c,\*</sup>

<sup>a</sup> Beckman Institute for Advanced Science and Technology, University of Illinois at Urbana-Champaign, Urbana, IL 61801 USA

<sup>b</sup> Department of Electrical and Computer Engineering, University of Illinois at Urbana-Champaign, Urbana, IL 61801 USA

<sup>c</sup> Department of Bioengineering, Chemical and Biomolecular Engineering, Mechanical Science and Engineering and University of Illinois Cancer Center, University of Illinois at Urbana-Champaign, Urbana, IL 61801 USA

An infrared spectrum recorded from a microscopic sample depends on spectral properties of the constituent material as well as on morphology. Many samples or domains within heterogeneous materials can be idealized as spheres, in which both scattering and absorption from the three-dimensional shape affect the recorded spectrum. Spectra recorded from such objects may be altered to such an extent that they bear little resemblance to spectra recorded from the bulk material; there are no methods, however, to reconcile the two from first principles. Here we provide the mathematical description of the optical physics underlying light-spherical sample interaction within an instrument. We use the developed analytical expressions to predict recorded data from spheres using Fourier transform infrared (FT-IR) spectroscopic imaging. Recorded spectra are shown to depend strongly on the size of the sphere as well as the optical arrangement of the instrument. Next, we present theory and experiments demonstrating the recovery of the complex refractive index of the material using data recorded from a sphere. The effects of the sample morphology on the measured spectra can be removed, and using the imaginary part of the index, the shape-independent IR absorption spectrum of the material is recovered.

Index Headings: Fourier transform infrared (FT-IR); Spectroscopic imaging; Sphere; Mie scattering; Theory; High-definition; Focal plane array; Correction; Algorithm; Forward problem; Inverse problem; Distortion; Morphology.

## INTRODUCTION

Infrared microspectroscopy and spectroscopic imaging are both in common use for the analysis of microscopically heterogeneous materials.<sup>1</sup> In these techniques, both the molecular content and structure on a microscopic scale are obtained without perturbing the sample. It has long been recognized, however, that scattering from domains within microscopically heterogeneous samples complicates interpretation of the recorded spectrum.<sup>2</sup> There has been renewed interest in understanding the dependence of recorded spectra on the structure of the samples, as summarized recently.<sup>3</sup> Observations have been reported both for heterogeneous materials in complex geometries as well as simple objects such as spheres. Unexplained differences between the spectrum of a material recorded from within a domain using a microscope and that expected from its refractive index have been previously described as errors or distortions initially<sup>4,5</sup> but are now recognized to arise from light-matter interactions specific to the sampling geometry and sample morphology. These observations have naturally sparked interest in recover-

ing the absorption spectrum of the material from recorded data such that the recovered spectra are independent of the sample morphology.<sup>4,6-8</sup> One set of approaches today seeks to model the material as an idealized object, such as a sphere, and largely neglects the optical configuration of the microscope and spectrometer. Success has been reported in using this approach to understand the spectra of complex tissues as well as that of spheres themselves.<sup>9,10</sup>

In another line of inquiry, a complete understanding of the recorded spectra has been sought from rigorous electromagnetic optical theory.<sup>11,12</sup> The propagation of light through the interferometer and microscope as well as the interactions with the sample are described analytically. Analysis for simple sample geometries, including multilayer planar structures and defined objects such as fibers,<sup>13</sup> has been reported. The dependence of the recorded data on the geometry of the sample could be explicitly modeled, and results indicated that the recorded data both from planar samples and cylinders could be used to recover the absorption spectrum of the material. A comprehensive theoretical description, predictions of recorded data, and experimental validation for measurements of a sphere using an infrared microscope, however, are lacking. While planar substrates can be understood as a series of one-dimensional (1D) structures, fibers are essentially two-dimensional (2D) in that the direction of the fiber axis does not provide any changes in material properties. Spheres are fully three-dimensional (3D) objects. Hence, attempts to understand the spectral data recorded from spheres is not a simple extension from previous work but represents a necessary advance to complete our understanding of 1D to 3D objects. A complete theoretical description and experimental validation for the same has not been reported.

Here we report on the development and validation of an analytically rigorous approach to IR microspectroscopy of spheres. We first present the theoretical framework for the forward model, incorporating the optical instrument, scattering, and absorption, to understand recorded data from spheres of known shape and spectral properties. This development is necessary to understand the effect of samples and optical configurations on the recorded data. The forward model is employed to illustrate the effects of instrumental parameters on data that would be recorded for specific spheres. As a second step, we also report here the development of an algorithm to reconstruct the spectral response of the bulk material comprising the spheres based on the solution of the inverse problem for the forward model. This development is necessary to recover the absorption spectrum of the material from data recorded from spheres using a specific instrumental configuration. The predictions and solutions of the inverse problem are

Received 4 September 2012; accepted 18 January 2013.

\* Author to whom correspondence should be sent. E-mail: rxb@illinois.edu.

DOI: 10.1366/12-06847

validated experimentally using Fourier transform infrared (FT-IR) microspectroscopic measurements.

## FORWARD MODEL

We first report on the forward model, where the aim is to understand the effects of known optical configurations and spherical objects on the data that would be recorded. There are two aspects to analyzing spectra recorded from spheres. The optical configuration must be modeled, and the properties of the sphere must be integrated into the optical system model. Classical optical theory provides a means to describe both the optical configuration as well as the interaction between focused light and a sphere with known radius and optical properties. The optical properties of the sphere depend on the wavenumber,  $\bar{\nu}$ , and are encoded in the complex refractive index,  $n(\bar{\nu}) = \eta(\bar{\nu}) + i\kappa(\bar{\nu})$ . The imaginary part,  $\kappa(\bar{\nu})$ , quantifies absorption and is of primary interest in the recovery of absorption spectra from recorded data.

For simplicity, we invoke the use of scalar fields in our analysis, but the analysis is readily generalized to vector fields. The incident field consists of a superposition of plane waves  $e^{i2\pi\bar{\nu}\mathbf{s}\cdot\mathbf{r}}$ , summed over all directions  $\mathbf{s}$  that lie within the solid angle of the focusing optics, i.e., Debye focusing.<sup>14,15</sup> For a single plane wave, choosing the  $z$  axis along the direction of  $\mathbf{s}$  and applying the partial wave expansion<sup>16</sup> of the plane wave, one obtains

$$e^{i2\pi\bar{\nu}\mathbf{s}\cdot\mathbf{r}} = \sum_{l=0}^{\infty} (2l+1) i^l j_l(2\pi\bar{\nu}r) P_l[\cos(\mathbf{s}\cdot\hat{\mathbf{r}})] \quad (1)$$

where  $j_l$  is the spherical Bessel function of the first kind,  $P_l$  represents the Legendre polynomials, and  $\hat{\mathbf{r}}$  is a unit vector in the direction of  $\mathbf{r}$ . Using the addition theorem of the spherical harmonics it is possible to write the total incident field as<sup>17</sup>

$$U_{\text{inc}}(\mathbf{r}, \bar{\nu}) = \sum_{l=0}^{\infty} \alpha_l j_l(2\pi\bar{\nu}r) P_l[\cos(\theta)] \quad (2)$$

where  $\theta$  is the angle between the direction  $\hat{\mathbf{r}}$  and the  $z$  axis.  $\alpha_l$  is defined as

$$\alpha_l = 2\pi i^l (2l+1) \int_b^a P_l[\cos(\theta_s)] \sin(\theta_s) d\theta_s \quad (3)$$

where  $\theta_s$  is the angle between the vector  $\mathbf{s}$  and  $\mathbf{z}$  and the integration limits depend on the optical properties of the focusing optics. The condenser is a Schwarzschild objective, with a numerical aperture of  $\text{NA}_c$  and an obscuration with a numerical aperture given by  $\text{NA}_{\text{cob}}$  then  $b$  equals  $\arccos[\sin(\text{NA}_c)]$  and  $a$  is  $\arccos[\sin(\text{NA}_{\text{cob}})]$ . The total field can be written as

$$U(r, \theta) = \begin{cases} U_{\text{int}}(r, \theta) & \text{if } r \text{ is inside a scatterer} \\ U_{\text{inc}}(r, \theta) + U_{\text{scat}}(r, \theta) & \text{if } r \text{ is outside a scatterer} \end{cases} \quad (4)$$

where  $U_{\text{int}}$  is the field inside an object,  $U_{\text{inc}}$  is the incident field, and  $U_{\text{scat}}$  is the scattered field due to the presence of the sphere. The internal and scattered fields can be formulated using a

local spherical basis as

$$U_{\text{int}}(\mathbf{r}, \bar{\nu}) = \sum_{l=0}^{\infty} A_l j_l(2\pi\bar{\nu}n(\bar{\nu})r) P_l[\cos(\theta)]$$

$$U_{\text{scat}}(\mathbf{r}, \bar{\nu}) = \sum_{l=0}^{\infty} B_l h_l^{(1)}(2\pi\bar{\nu}r) P_l[\cos(\theta)] \quad (5)$$

where  $h_l^{(1)}$  is the spherical Hankel function.

Enforcing the appropriate boundary conditions allows the determination of the coefficients  $A_l$  and  $B_l$ .\*

Here, the appropriate boundary conditions arise from conservation dictating that the sum of the incident plane wave, scattered field, and the internal field must be continuous and have a continuous first derivative. This formulation makes it possible to explicitly calculate the scattered field resulting from each plane wave incident on a single sphere, a multilayered sphere, or a collection of spheres. The total fields can be calculated by summing the contributions from all the plane waves that lie within the solid angle of the focusing optics. The fields resulting in the focused illumination of a sphere are shown in Fig. 1. It should be noted that, in the interest of describing field interactions with a sphere, this simulation does not include a substrate on which the sphere may be resting in an actual experiment. The effect of a transmitting substrate would be relatively small, contributing only a very small fraction of backscattered light from the sphere, which would then be inefficiently reflected and interact again with the sphere. The results will likely change only by a fraction of a percent in the simulation here, and the effect of the substrate would not be visible, even if it were included.

Asymptotic expressions are used for the spherical Hankel functions and for the incident plane waves, i.e.,  $h_l^{(1)}(x) \rightarrow \frac{\exp[i(x-l\pi/2)]}{ix}$  and  $\exp(i\mathbf{k}\cdot\mathbf{r}) \rightarrow \frac{2\pi}{ikr} \delta(\hat{\mathbf{k}} - \hat{\mathbf{r}})$ <sup>17,18</sup> The detection process is approximated as an integration of the optical intensity over the detection aperture,

$$I(\mathbf{r}, \bar{\nu}) = \iint |U(r, \theta, \bar{\nu})|^2 r^2 \sin(\theta) dr d\theta \quad (6)$$

The imaging system modeled here consists of a Schwarzschild focusing objective and an opposing condensing lens of similar geometry but not necessarily of the same numerical aperture or obscuration, and is illustrated in Fig. 2A. The condensing objective has a numerical aperture of  $\text{NA}_c$  and an obscuration with a numerical aperture given by  $\text{NA}_{\text{cob}}$ . Likewise, the detection lens can be described by  $\text{NA}_d$  and  $\text{NA}_{\text{dob}}$ . The intensity at the detector is recorded with,  $I_S(\mathbf{r}, \bar{\nu})$ , and without,  $I_0(\mathbf{r}, \bar{\nu})$ , the sphere to yield the recorded absorbance,  $A(\mathbf{r}, \bar{\nu})$ , given by

\* The coefficients are given by

$$A_l = \alpha_l \frac{h_l^{(1)}(2\pi\bar{\nu}a) j_l(2\pi\bar{\nu}a) - h_l^{(1)}(2\pi\bar{\nu}a) j_l'(2\pi\bar{\nu}a)}{h_l^{(1)}(2\pi\bar{\nu}a) j_l[2\pi\bar{\nu}n(\bar{\nu})a] - n(\bar{\nu}) h_l^{(1)}(2\pi\bar{\nu}a) j_l'[2\pi\bar{\nu}n(\bar{\nu})a]},$$

$$B_l = \alpha_l \frac{n(\bar{\nu}) j_l(2\pi\bar{\nu}a) j_l'(2\pi\bar{\nu}na) - j_l[2\pi\bar{\nu}n(\bar{\nu})a] j_l'(2\pi\bar{\nu}a)}{h_l^{(1)}(2\pi\bar{\nu}a) j_l[2\pi\bar{\nu}n(\bar{\nu})a] - n(\bar{\nu}) h_l^{(1)}(2\pi\bar{\nu}a) j_l'[2\pi\bar{\nu}n(\bar{\nu})a]},$$

where the prime indicates differentiation with respect to the argument in parentheses.

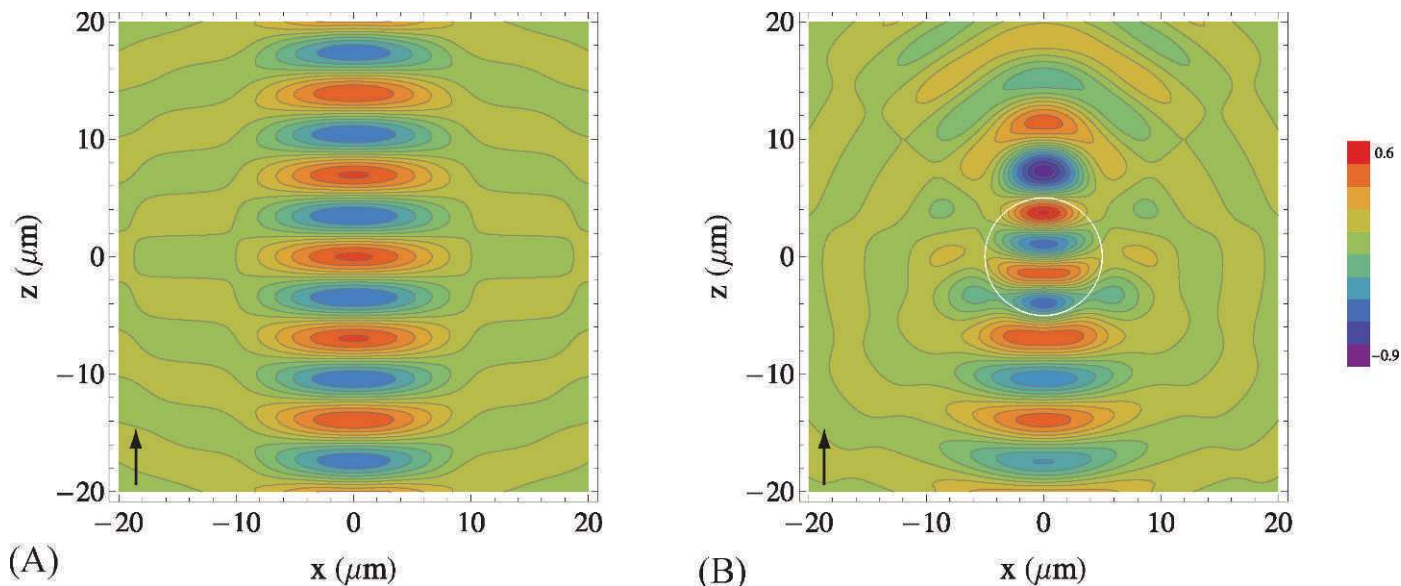


FIG. 1. Illustration of the real parts of the fields (A) in a microscope with no sample and (B) inside and outside a sphere when it is illuminated with a field focused at the center of the sphere. The sphere has a radius of  $5\ \mu\text{m}$  and is made of PMMA, and the illumination is at  $1500\ \text{cm}^{-1}$ . The arrow indicates direction of propagation.

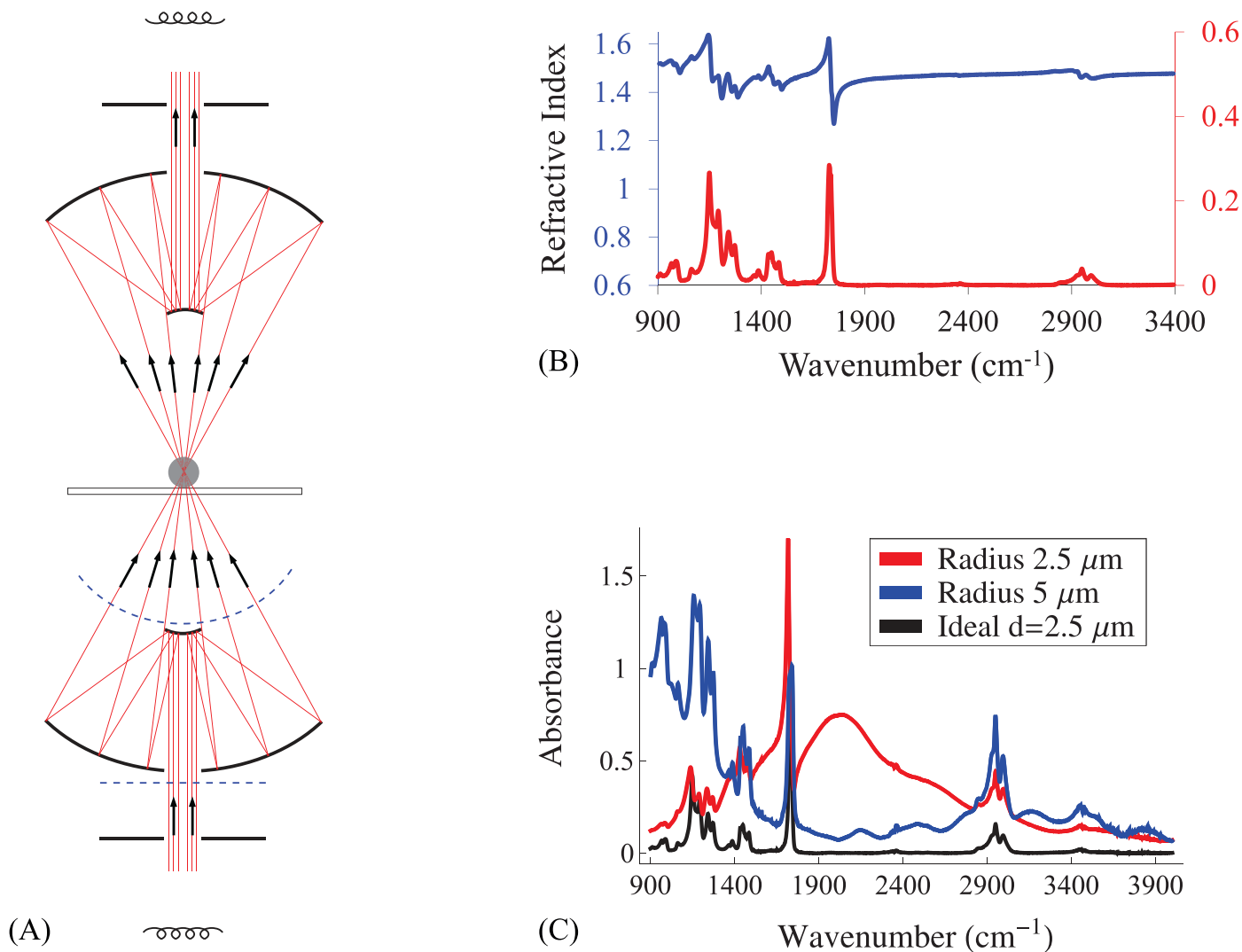


FIG. 2. (A) Illustration of the focusing transmission optics. (B) The refractive index of PMMA, obtained from recording data from a slab of PMMA. (C) Predicted data for a PMMA sphere with radii of  $2.5\ \mu\text{m}$ ,  $5\ \mu\text{m}$ , and for an ideal sample of thickness  $d = 2.5\ \mu\text{m}$ .

$$A(\mathbf{r}, \bar{\nu}) = -\log_{10} \left[ \frac{I_S(\mathbf{r}, \bar{\nu})}{I_0(\mathbf{r}, \bar{\nu})} \right] \quad (7)$$

Beer's law relates the spectrum to the imaginary part of the refractive index of the sample and the sample path length,  $d$ , by

$$A(\bar{\nu}) = \frac{4\pi\bar{\nu}\kappa(\bar{\nu})d}{\log_e(10)} \quad (8)$$

For a sample that can be treated as a slab, the path length is simply the thickness of the sample. The expression above for calculating the absorbance from measurements neglects boundary phenomena at the sample, including diffraction and elastic scattering, and is strictly valid for a single plane wave. In a microscope, even for simple samples, the measured absorbance is not given by the thickness of the slab due to both sample boundaries as well as the angular diversity inherent in focusing. Instead, the recorded data are coupled to the slab geometry.<sup>12</sup> All these effects are relevant in the case of measurements of spheres, especially where the size of the spheres is on the order of the illuminating wavelengths.

**Predictions of Recorded Data.** We apply the forward model developed above to predict the recorded absorption spectrum for poly(methyl methacrylate) (PMMA) spheres in an IR microscope. The refractive index of PMMA (Fig. 2B) is obtained by recording data from a film (slab geometry) of PMMA, whose thickness was characterized using ellipsometry and FT-IR microscopy as detailed in the experimental section. Using the microscope model and data, we simulated data that would be recorded for different-sized spheres. Absorption spectra that would be recorded for PMMA spheres with radii of 2.5  $\mu\text{m}$  and 5  $\mu\text{m}$  are plotted in Fig. 2C. Several trends are obvious in these predictions. The imaginary part of the refractive index strongly influences the measured absorbance, as is expected from Beer's law. Mie scattering, however, strongly couples the real and the imaginary parts of the refractive index in the measured absorbance. Compared with an ideal slab, the spectrum that would be recorded from spheres can be seen to additionally depend on the size of the sphere and the parameters of the imaging system. We emphasize here that this dependence should not be called a distortion or an artifact. It is simply the consequence of coupling between molecular and morphological properties of the sample. In fact, the spectra become richer in information, since this traditionally molecular measurement now encodes structure as well. While the morphologic information regarding spherical domains inherent in spectra has been previously noted and can be used,<sup>19,20</sup> there has not previously been a deterministic relationship between the properties of the sample and the recorded spectrum. Figure 2C provides an example of the same and should be valuable for measurements, in a microscope, of a range of polymers domains and objects, aerosols, and forensic samples.

While the dependence of the recorded spectra on the size of the sphere is expected and has been observed in past studies, a less appreciated aspect is the effect of the optical system on the recorded data. Though previous studies have reported changes in spectra as a result of the sampling configuration (e.g., transmission versus transmission–reflection configurations), the dependence of recorded data on changing the optical properties of a single sampling configuration have not been discussed. It is important to note that the measured spectra depend greatly on the parameters of the imaging system, as is illustrated in Fig. 3. Here, the NA of the objective is the only quantity that is

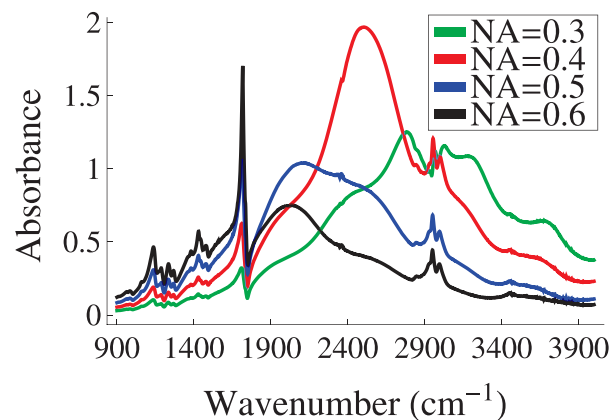


FIG. 3. Predicted data for a PMMA sphere with a radius of 2.5  $\mu\text{m}$  for four different numerical apertures.

changed, demonstrating the dramatic effect of using different lenses. While a complete discussion of the optical system and its effects on the recorded data from spheres is not presented here, the developed theory can be used for such modeling. Figure 3 is an important result both from a practical standpoint for applied spectroscopists as well as an early suggestion to focus attention on the optical configuration when attempting to recover sample properties from recorded data. To our knowledge, none of the empirical scattering-based methods seeking to recover correct absorption data have thus far accounted for the optical configuration of their instrument. In the next section, we invoke both the scattering from the sphere as well as the influence of the optical configuration in solving the inverse problem.

**Inverse Problem and Its Solution.** The interaction between the sphere and focused light is described using the forward model detailed above. Given the size of the sphere and the parameters of the optical setup, the spectrum that would be recorded can be predicted in the forward model. While the development is useful for fundamental studies, a practical task is to predict the structure and properties of the sphere from the recorded data. Hence, this forward model has to be inverted to recover the spectral properties and diameter of the sphere. The inversion is done by finding the properties of the sphere that result in a prediction of the recorded spectrum from the forward model that best fits the measured spectrum. In this paradigm, the index of refraction, size of the sphere, and the optical properties of the imaging system are the parameters. The optical properties of the imaging system are usually provided by the manufacturer or can be determined from independent measurements. We caution, however, that the reported values from the manufacturer are approximate, and an accurate assignment of values would provide more accurate results for specific configurations. Figure 3 provides an illustration of the strong dependence of recorded data on the optical configuration, implying that an accurate assessment of the same is needed for accurately solving the inverse problem. Hence, we first determined the values of the optical properties in our particular setup using spheres of known size. The approach described below provides a means to make fine adjustments to the manufacturer's values in a self-consistent manner.

The real and imaginary parts of the refractive index are related (Kramers–Kronig relations); hence, it is not ordinarily possible to deduce the real part of the refractive index just from

**TABLE I.** Experimental parameters used for data acquisition and modeling.

| Parameter  | Value |
|------------|-------|
| $NA_c$     | 0.5   |
| $NA_{cob}$ | 0.23  |
| $NA_d$     | 0.65  |
| $NA_{dob}$ | 0.23  |

a measurement of absorption bands. Most organic materials of interest, however, have a large zero-absorbance zone between  $2100\text{ cm}^{-1}$  and  $2600\text{ cm}^{-1}$  (correcting for atmospheric  $\text{CO}_2$ ). We employ this region to calculate the real part of the refractive index accurately ( $\eta_0$ ). The four NA values associated with the image formation optics and the radius of the sphere can then be found by minimizing the mean square error between the prediction using a set of parameters [ $n(\bar{\nu}) = \eta_0$ ,  $\kappa(\bar{\nu}) = 0$ ,  $NA_c$ ,  $NA_{cob}$ ,  $NA_d$ ,  $NA_{dob}$ ] and the recorded data in the zero-absorbance zone (Table I). The real part of the index in other parts of the spectrum and the corresponding imaginary part can then be calculated in other spectral regions using the determined values of the optical system and radius of the sphere as well as the constant value of the refractive index. The iterative scheme to recover the complex refractive index using minimizing the difference between the recorded,  $A(\mathbf{r}, \bar{\nu})$ , and the predicted absorbance,  $A_{\text{pred}}[\mathbf{r}, \bar{\nu}, \eta(\bar{\nu}), \kappa(\bar{\nu})]$ , similar to that of Ref. 13 in principle but includes the specifics of scattering from a sphere. A bracketed superscript denotes the iteration number.

**Initialize.** Set the initial index estimate to  $n^{(0)} = \eta_0$ . Initialize the iteration counter  $j = 0$ .

**Predict.** Calculate the predicted data  $A^{(j)}(\mathbf{r}, \bar{\nu}, \eta^{(j)}(\bar{\nu}), \kappa^{(j)}, \bar{\nu})$ .

**Difference.** Evaluate the difference.

$$E^{(j)}[\bar{\nu}, \eta^{(j)}(\bar{\nu}), \kappa^{(j)}(\bar{\nu})] = A(\mathbf{r}, \bar{\nu}) - A^{(j)}[\mathbf{r}, \bar{\nu}, \eta^{(j)}(\bar{\nu}), \kappa^{(j)}(\bar{\nu}), \bar{\nu}] \quad (9)$$

**Update.**

(a) Update the imaginary part of the complex refractive index as

$$\kappa^{(j+1)}(\bar{\nu}) = \kappa^{(j)}(\bar{\nu}) + \frac{\log_e(10)}{4\pi\bar{\nu}(2R)} E^{(j)}[\bar{\nu}, \eta^{(j)}(\bar{\nu}), \kappa^{(j)}(\bar{\nu})] \quad (10)$$

(b) Set any negative values of  $\kappa^{(j+1)}(\bar{\nu})$  to zero.

(c) Update the real part of the complex refractive index as

$$\eta^{(j+1)}(\bar{\nu}) = \eta_0 + KK[\kappa_{(j+1)}(\bar{\nu})] \quad (11)$$

where KK indicates the Kramers–Kronig relation.

**Iterate.** Increment the iteration counter  $j \rightarrow j + 1$ , or stop the algorithm if it has converged.

The algorithm is initialized with  $\eta = \eta_0$ ,  $\kappa = 0$ , and optical properties obtained from optimizing the forward model in the zero-absorbance region. For each iteration, a prediction of the absorption spectrum for the current value of the refractive index is obtained. The difference between this prediction and the measured absorbance is then used to update the imaginary part of the refractive index. The scaling factor that is present in Eq. 10 to relate the imaginary part of the index to the

absorbance determines the step size by which the imaginary part is updated. The value of this constant is motivated by the expression for the absorbance from an ideal planar sample with a thickness equal to the diameter of the sphere. After the update of the imaginary part of the refractive index, any negative values are set to zero, since a negative refractive index represents the creation of energy and has no physical possibility. Based on the updated imaginary refractive index, the real part can also be updated using a discrete implementation of the Kramer–Kronig relation.<sup>21</sup>

## EXPERIMENTAL

Poly(methyl methacrylate) microspheres were obtained from Cospheric, Santa Barbara, CA, with a diameter between 5 and 20  $\mu\text{m}$ . A small volume of spheres were dispersed onto a 2.5 mm thick barium fluoride ( $\text{BaF}_2$ ) substrate by gently tapping a loaded pipette tip, and regions with individual spheres on the substrate were found. A visible microscope, Zeiss Axio Imager.M2 (Carl Zeiss AG, Oberkochen, Germany), was used to record visible images and determine sizes of spheres prior to recording IR imaging data. IR imaging data were recorded using an imaging spectrometer consisting of a Varian 7000 FT-interferometer (Agilent, Mississauga, Ontario, Canada) coupled to a UMA-400 microscope (Digilab, Marlborough, MA). The system was equipped with a  $128 \times 128$  pixel mercury–cadmium–telluride focal plane array detector that was used for imaging. The commercially available detection Schwarzschild objective (NA = 0.5) was replaced with a higher NA (0.65, 74 $\times$ ) objective with an obscuration of NA = 0.23.<sup>22</sup> Spectra were recorded at  $4\text{ cm}^{-1}$  resolution at an undersampling ratio of 4 in rapid scanning mode. Data were Fourier transformed, and a single beam imaging set from an adjacent, sphere-free region was used to calculate absorption spectra using a pixel-for-pixel ratio. The spheres were dissolved in Toluene and cast a film on  $\text{BaF}_2$  substrates. IR and ellipsometric measurements (Rudolph FE-III Focus ellipsometer, Entrepix, Phoenix, AZ) were conducted to determine the refractive index of PMMA.

## RESULTS AND DISCUSSION

Spectra from a number of PMMA spheres ( $>20$ ) were recorded using the imaging system. We use the imaging data to select the center pixel of each sphere, since this is the pixel for which the present formulation is most valid. We do not use the remainder of the data and focus instead on extracting the absorption spectrum for this consistent case across spheres of different sizes. The algorithm is validated by comparing the reconstructed refractive index to the actual refractive index of PMMA. The described algorithm was applied to the data shown in Fig. 4A and Fig. 4D. The results of the reconstruction are shown in Figs. 4B–C and Figs. 4E–F. It can be seen that the recovered refractive index provides a close match between the measurement and the predicted data. Thus, the described theory is capable of describing recorded data. The estimate of the refractive index also follows the bulk material properties closely. The retrieved refractive index differs from the true value especially at the strongest absorption peak and at the edges of the spectral bandpass. While the strong absorption mismatch arises from the fitting of the data emphasizing the entire spectrum at the expense of isolated strong peaks, the edge mismatch arises from the finite spectral range available from the Kramers–Kronig transform. It must also be noted that

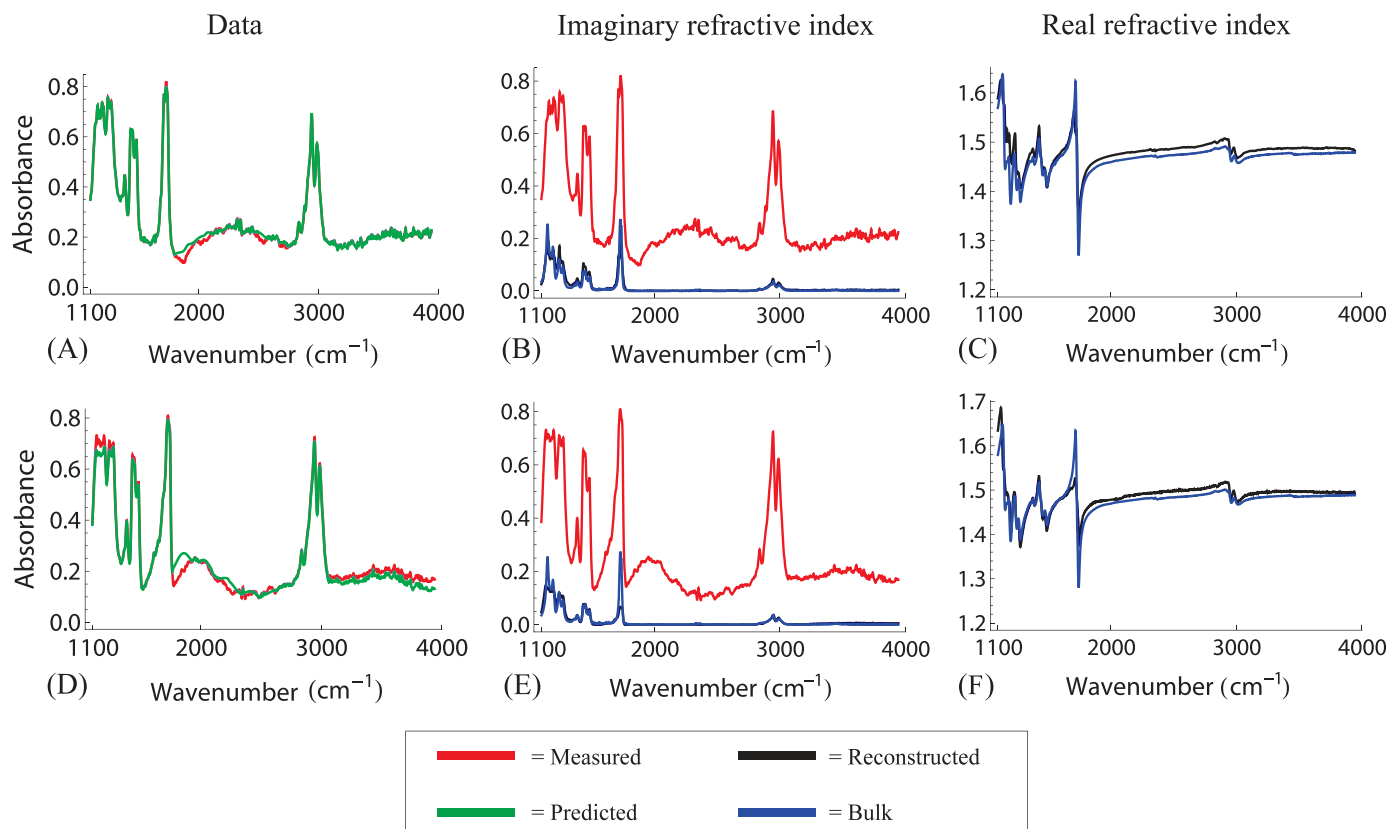


FIG. 4. Reconstructions and true, or bulk, values of the complex refractive index and the corresponding measured data and predicted data with the reconstructed refractive index as input. Sphere with a radius of  $6.5 \mu\text{m}$  (A–C) and sphere with a radius of  $8.5 \mu\text{m}$  (D–F) are considered. The reconstructions are produced after 10 iterations of the algorithm.

the data are of reasonable, but not exceptional, signal-to-noise ratio. The reconstruction appears to not be significantly affected by noise, even at these levels that are easily attained in most experiments. Thus, the proposed algorithm is reasonably accurate and likely applicable to most data acquired at the present time with commercially available microscopy systems.

This manuscript presents a complete forward model and an inverse solution for data recorded from spheres. The validation of the developed model with experiments demonstrates the potential for this approach in recovering absorption data after removing the effects of the sample's structure. The results also highlight several areas for improvement. The recovery of accurate absorbance is likely complicated for strong, isolated, and sharp bands due to the trade-off in fitting the entire spectrum versus local features. Hence, improved algorithms for better fitting are one area for future development. The limited bandwidth of the recorded spectrum is also a constraint, leading to poorer fitting at the spectral edges of the recorded data. While limited data are usually acquired to minimize storage and improve the signal-to-noise ratio for a given acquisition time, the results here indicate that the need for reconstruction accuracy may dictate larger bandwidth detectors or extended spectral range acquisition. Considering the center pixel allows a careful analysis and reconstruction of the spectrum for the case where light is focused at the center of the sphere. This is merely the first milestone problem to be solved in the general case of understanding spheres, multiple spheres, and models of samples as spheres. Hence, considerable

opportunity exists for further modeling and refinement. The basic theoretical framework for the same is provided by this manuscript. The framework and approach reported, finally, are also entirely compatible with what may be recorded using an aperture-based single point microscopy system. We have concentrated on the case that a sphere is centered with respect to the objective and condenser as well as at the axial plane of the focus of the microscope. This case forms the core of the theoretical framework to understand all cases of spheres, whether at the focus or defocused, centered in the field of view, or to the side, as well as ensembles of spheres. We have not presented the wide-field imaging case or the case of multiple, optically coupled spheres, though the theory generalizes to those cases in a straightforward manner.

## CONCLUSIONS

We have presented a theoretical model for the light–matter interaction in an IR microscope for the case of spheres. Morphology and molecular composition are necessarily comingled in the acquisition of data from such heterogeneous samples. Predictions for the recorded data were made for a given optical system and spheres with known material properties. Predicted data agreed with recorded observations. An algorithm to solve the inverse problem was presented to extract the complex refractive index of the spheres from data, and the index, in turn, was employed to compute the size-independent bulk absorption spectrum. This experimental demonstration of the separate determination of shape (in the form of the sphere radius) and spectroscopic response should

provide a framework to recover spectra from spheres routinely, as well as a starting point for models of more complex samples.

#### ACKNOWLEDGMENTS

The authors would like to thank Beomjin Kwon for performing the ellipsometry measurements on the slab of PMMA. Funding from the Beckman Fellows program, the National Science Foundation (via grant CHE 0957849), and the National Institute of Health (via grant RO1CA38882) is gratefully acknowledged.

1. I.W. Levin, R. Bhargava. "Fourier Transform Infrared Vibrational Spectroscopic Imaging: Integrating Microscopy and Molecular Recognition". *Ann. Rev. Phys. Chem.* 2005. 56: 429-474.
2. R. Bhargava, S.Q. Wang, J.L. Koenig. "FT-IR Imaging of the Interface in Multicomponent Systems Using Optical Effects Induced by Differences in Refractive Index". *Appl. Spectrosc.* 1998. 52(3): 323-328.
3. R. Bhargava. "Infrared Spectroscopic Imaging: The Next Generation". *Appl. Spectrosc.* 2012. 66(10): 1091-1120.
4. B. Mohlenhoff, M. Romeo, M. Diem, B.R. Woody. "Mie-Type Scattering and Non-Beer-Lambert Absorption Behavior of Human Cells in Infrared Microspectroscopy". *Biophys. J.* 2005. 88(5): 3635-3640.
5. J. Lee, E. Gazi, J. Dwyer, M.D. Brown, N.W. Clarke, J.M. Nicholson, P. Gardner. "Optical Artefacts in Transection Mode FTIR Microspectroscopic Images of Single Cells on a Biological Support: The Effect of Back-Scattering into Collection Optics". *Analyst.* 2007. 132(8): 750-755.
6. H. Martens, J.P. Nielsen, S.B. Engelsen. "Light Scattering and Light Absorbance Separated by Extended Multiplicative Signal Correction. Application to Near-Infrared Transmission Analysis of Powder Mixtures". *Anal. Chem.* 2003. 75(3): 394-404.
7. A. Kohler, C. Kirschner, A. Oust, H. Martens. "Extended Multiplicative Signal Correction as a Tool for Separation and Characterization of Physical and Chemical Information in Fourier Transform Infrared Microscopy Images of Cryo-Sections of Beef Loin". *Appl. Spectrosc.* 2005. 59(6): 707-716.
8. A. Kohler, J. Sule-Suso, G.D. Sockalingum, M. Tobin, F. Bahrami, Y. Yang, J. Pijanka, P. Dumas, M. Cotte, D.G. van Pittius, G. Parkes, H. Martens. "Estimating and Correcting Mie Scattering in Synchrotron-Based Microscopic Fourier Transform Infrared Spectra by Extended Multiplicative Signal Correction". *Appl. Spectrosc.* 2008. 62(3): 259-266.
9. P. Bassan, H.J. Byrne, F. Bonnier, J. Lee, P. Dumas, P. Gardner. "Resonant Mie Scattering in Infrared Spectroscopy of Biological Materials—Understanding the 'Dispersion Artefact'". *Analyst.* 2009. 134(8): 1586-1593.
10. P. Bassan, A. Kohler, H. Martens, J. Lee, E. Jackson, N. Lockyer, P. Dumas, M. Brown, N. Clarke, P. Gardner. "RMieS-EMSC Correction for Infrared Spectra of Biological Cells: Extension Using Full Mie Theory and GPU Computing". *J. Biophotonics* 2010. 3(8–9): 609-620.
11. B.J. Davis, P.S. Carney, R. Bhargava. "Theory of Mid-infrared Absorption Microspectroscopy: II. Heterogeneous Samples". *Anal. Chem.* 2010. 82(9): 3487-3499.
12. B.J. Davis, P.S. Carney, R. Bhargava. "Theory of Mid-Infrared Absorption Microspectroscopy: I. Homogeneous Samples". *Anal. Chem.* 2010. 82(9): 3474-3486.
13. B.J. Davis, P.S. Carney, R. Bhargava. "Theory of Infrared Microspectroscopy for Intact Fibers". *Anal. Chem.* 2011. 83(2): 525-532.
14. P. Debye. "Das Verhalten von Lichtwellen in der Nähe eines Brennpunktes oder einer Brennlinie". *Ann. Phys.* 1909. 335(14): 755-776.
15. E. Wolf, Y. Li. "Conditions for the Validity of the Debye Integral Representation of Focused Fields". *Opt. Commun.* 1981. 39(4): 205-210.
16. H.C. van de Hulst. "Licht Scattering by Small Particles". Dover Publications. 1982.
17. C.J. Joachain. "Quantum Collision Theory". Elsevier Science Ltd. 1984. 3<sup>rd</sup> ed.
18. P.G. Mulligan, D.S.F. Crothers. "Plane Wave and Coulomb Asymptotics". *Phys. Scripta.* 2004. 70(1): 17-20.
19. R. Bhargava, S.Q. Wang, J.L. Koenig. "Studying Polymer-Dispersed Liquid-Crystal Formation by FTIR Spectroscopy. 1. Monitoring Curing Reactions". *Macromolecules.* 1999. 32(26): 8982-8988.
20. R. Bhargava, S.Q. Wang, J.L. Koenig. "Studying Polymer-Dispersed Liquid-Crystal Formation by FTIR Spectroscopy. 2. Phase Separation and Ordering". *Macromolecules.* 1999. 32(26): 8989-8995.
21. A.B. Kuzmenko. "Kramers-Kronig Constrained Variational Analysis of Optical Spectra". *Rev. Sci. Instrum.* 2005. 76(8): 083108.
22. R.K. Reddy, M.J. Walsh, M.V. Schulmerich, P.S. Carney, R. Bhargava. "High-Definition Infrared Spectroscopic Imaging". *Appl. Spectrosc.* 2013. 67(1): 93-105.